ULTRASONIC IMAGING 7, 277-292 (1985)

SPECULAR REFLECTOR NOISE : EFFECT AND CORRECTION FOR IN VIVO ATTENUATION ESTIMATION

P. Laugier[1], G. Berger[1], M. Fink[1,2] and J. Perrin[1]

[1]Laboratoire de Biophysique UA 593
CHU Cochin Port-Royal
24, Rue du Faubourg Saint-Jacques
75674 PARIS CEDEX 14, FRANCE

[2]Groupe de Physique des Solides
2, Place Jussieu
75005 PARIS, FRANCE

After reviewing the usual models proposed for the echographic response of soft tissues, we discuss the interaction between the ultrasonic wave and large size obstacles. Structures of this size, specular reflectors, can be found in tissues. The influence of such reflectors on in vivo attenuation measurements is detailed. We point out the importance of the specular echo noise originating from two kinds of reflectors : plane-like and vessel-like reflectors. We present a complete study of their influence on two different algorithms for attenuation estimates : the spectral centroid shift and the narrow band methods. Results are presented on stimulated data, a tissue-mimicking phantom and in vivo muscle data. Different procedures for minimizing the specular echo noise are also discussed.

Key words : Attenuation ; muscle ; specular reflector ; tissue characterization ; tissue model ; ultrasound.

I. INTRODUCTION

Different in vivo techniques have been investigated in order to provide quantitative information on soft tissues. Attenuation appears to be one of the promising quantitative parameters for tissue characterization. Many results are available in the literature, especially on liver, which is the most frequently explored organ [1-3], but also on muscle tissue [4].

Algorithms for evaluating in the reflection mode the slope of the attenuation versus frequency have been reported by many authors. As attenuation in tissue is frequency dependent [5-8], the amount of energy received by the probe is a function of both frequency and depth. Attenuation acts as a time-varying frequency filter. For this reason, most of the algorithms are based on the calculation of the power spectra of the windowed rf signal. Short time Fourier analysis allows the use of the totality of data points and provides a representation of energy density vs. time and frequency [9,10].

However, one of the major problem encountered while measuring attenuation is diffraction. It has been shown that dif-

0161-7346/85 $3.00

fraction also acts as a time-varying frequency filter, and so yields a biased attenuation slope value. This effect is particularly important with focused probes [10-13]. Methods for correcting this effect have been proposed but up to now do not appear to be applicable for in vivo data. Nevertheless, if special precautions are taken, it is possible to standardize the measurement and to obtain comparable and relative attenuation values in one organ. The precautions consist of using the same probe and placing the explored organ in the same part of the acoustic field.

In addition, the frequency content of the signal depends on the scattering properties of the tissue. This paper shows that besides the diffraction, time-varying, frequency filter there is a scattering, time-varying frequency function related to the degree of inhomogeneity in real tissue. Such an effect, due to the presence in tissue of any large scatterer (i.e., no longer considered as a point-like scatterer), may introduce a bias into the attenuation slope estimation. We call this frequency dependent effect "specular echo noise". We identified this effect on in vivo muscle (vastus medialis) [14]. As shown in this paper, the specular echo noise was identified with simulated rf signals which contain specular echoes and with tissue phantoms which include these types of reflectors. We present different procedures to minimize the specular echo noise.

II. THEORY

1) Tissue model

Biological tissue models proposed up to now, aiming at the representation of the echographic signal, analyze tissues in term of multiscatterer media. The medium is represented as a random distribution of isotropic, point-like scatterers embedded in an homogeneous attenuation matrix. Under these conditions, the echographic signal results in the superposition of echoes from individual scaterrers, and is expressed by [13]

$$s(t) = g(t) * \iiint h2(\vec{M},t) * a2(\vec{M},t) * u(\vec{M},t)\ .d^3v, \quad (1)$$

where * means the convolution operation, $g(t)$ is a source dependent term, $h2(\vec{M},t)$ is the two-way diffraction impulse response (the diffraction filtering effect of diffraction has been detailed elsewhere [13] and thus is not discussed), and $a2(\vec{M},t)$ measures the attenuation effect whose transfer function in the frequency domain can be written as

$$A2(\tau,f) = \exp(-\beta f^n c\tau) \quad , \quad (2)$$

where βf^n is the attenuation law, n being nearly 1 for soft tissues. The function $u(\vec{M},t)$ is the scattering function for the differential volume d^3v which depends on the characteristics of the scatterers. The simplest case deals with a single point-like scatterer located at $\vec{Mo}$ for which

$$u(\vec{M},t) = \delta(\vec{M}-\vec{Mo})\ u(t) \quad , \quad (3)$$

The transfer function associated with u(t) is f^2 dependent (Rayleigh scatterer). For randomly distributed point-like scatterers, $u(\vec{M},t)$ can be written as

$$u(\vec{M},t) = \chi(\vec{M}) \quad u(t) \qquad , \tag{4}$$

where $\chi(\vec{M})$ represents the spatial distribution of the scatterers and u(t) the scattering amplitude for Rayleigh scatterers.

However, the random distribution of scatterers is not complete for the description of complex biological media. Tissues, such as muscle, include reflecting structures whose dimensions are large with respect to the ultrasonic wavelength. Hence, a more realistic model for the echographic signal should also include the interaction between the incident wave and structures such as specular reflectors. The scattering function for a specular reflector can be written in the form

$$u1_\theta(\vec{M},t) = \delta(\vec{M}-\vec{M}1) \; u1_\theta(t), \tag{5}$$

where θ is the orientation of the reflector with respect to the ultrasonic beam axis.

Although a specular reflector is wide and not point-like, we may consider for each echographic response that the effect of the specular reflector is local, around a mean position $\vec{M}1$ corresponding to its depth on the A-line. In the case of a specular reflector, the angular dependence of the scattering function must be noticed. However, it is not necessary to know explicitly the angular dependence because we shall be interested only in the mean frequency filtering effect. We just have to keep in mind that this filtering effect results in a double angle and frequency dependence of the scattering function. The scattering function $u1_\theta(t)$ is different from the response of a point-like scatterer. The amplitude and frequency content of the corresponding transfer function will be both modified. A plane reflector has a frequency independent response. Any intermediate case can be expressed in terms of f^p, the varying scattering transfer function with p ranging between 0 and 2 and depending upon the size of the reflector. The amplitude of the scattering function measures the deviation between the impedance of the reflector and the impedance of the surrounding medium.

In our simulations with specular reflectors, we shall consider both the amplitude and the frequency effects.

2) Short Time Fourier Analysis

The Short Time Fourier Analysis algorithm has been developed in order to estimate the frequency dependent attenuation with in vivo data. The rf signal is sampled by a sliding time window. For each position of the time window, the power spectrum is calculated. The change of the rf signal spectral content with depth, as shown in Eq. (1), is due to :

- the diffraction filter and the attenuation filter

- the scattering filter : in the case of randomly distributed scatterers, only the stochastic nature of backscattered

signals due to interferences between echoes from individual scatterers causes the scalloped power spectra. In order to smooth the spectra, many rf signals must be recorded by appropriate scanning and the spectra from identical depths must be averaged.

In the case of a specular reflector, the scattering function of the tissue slice containing the reflector be can written as $u(\vec{M},t) + u1_\theta(\vec{M},t)$ and the corresponding spectrum will result from stochastic (with $u(\vec{M},t)$) and deterministic (with $u1_\theta(\vec{M},t)$) processes. Because of its size, it may be possible for a specular reflector to be shared in common by several A-lines of one scan. As the time resolution of the running spectra vs. depth is limited by the time window duration (about 10 µs), it may occur that equivalent (i.e., equidistant) time windows on different A-lines will enclose the specular echo. As a consequence, the rf lines will correlate, due to the specular reflector. The importance of this correlation depends on the reflector size and orientation. Averaging the equidistant spectra smooths the spectra with respect to the random interferences noise, but may also result in enhancing the specular echo noise.

3) Estimation of the slope of attenuation

Our purpose is to study the bias introduced by the specular echo noise when estimating the slope of attenuation. We shall briefly recall the principle of two of the classical attenuation measurement techniques [8].

a) Spectral centroid shift

This method provides, from the running spectra, an estimation of the spectral centroid location with range. If the attenuation is assumed to be proportional to frequency and after the data have been corrected for diffraction (if not, only a relative value of the slope of attenuation is estimated) it may be shown that

$$\frac{df_c(\tau)}{d\tau} = -2\,\beta_0 c\,\sigma^2(\tau) \quad , \qquad (6)$$

with β_0 slope attenuation (dB/cm.MHz), c ultrasound velocity, $f_c(\tau)$ running spectral centroid and $\sigma^2(\tau)$ running spectral variance. The slope of attenuation is estimated from a linear fit of the running spectral centroid.

b) Narrow band

In this technique, the first step estimates the log-intensity decay with range at each individual sampled frequency value and a linear fit provides for the attenuation coefficient (dB/cm) at that frequency. The relation is

$$\frac{d}{d\tau}(\log S(\tau,f) = -0.868\,\beta f^n c \quad , \qquad (7)$$

where $S(\tau,f)$ is the running power spectra.

It is possible in a second step to plote the estimated values of attenuation coefficient (dB/cm) vs. frequency and a linear fit through the frequency-attenuation curve gives the slope of attenuation β_o (dB/cm.MHz).

III. INFLUENCE OF SPECULAR ECHOES IN A SPECTRAL CENTROID SHIFT METHOD

1) Simulation

We were interested in simulating two kinds of reflecting structures, which are found in biological tissues. We considered structures acting as a simple reflecting plane (connectives tissues), and as a double reflecting plane (vessels). The latter will originate a nonrandom interference noise.

Results are presented after averaging the equidistant power spectra corresponding to 32 different simulated A-lines. Figure 1a represents the running spectra (obtained using a Hamming window of 10.20 µs duration with 8.96 µs overlapping) in a simulated medium containing a plane-like reflector. The running spectra present a maximum of energy, corresponding to the reflector location, with enhancement of the low frequencies quite visible on the figure.

The vessel-like reflecting structure is shown on figure 1b. The scalloping pattern of the spectra is due to the deterministic interferences process resulting from the reflecting walls of the vessel-like structure.

The effect of these two reflector types on the running spectral centroid and variance is shown on figure 2. The correlation between the lines appears to be important due to the

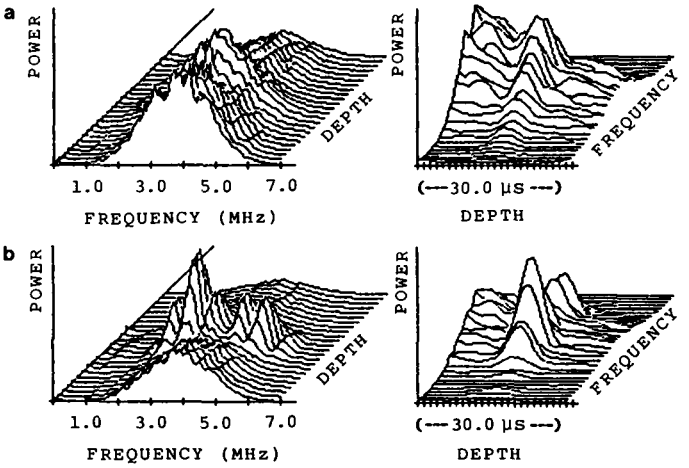

Fig. 1 Simulation : Running power spectra averaged on 32 simulated A-lines. (a) showing the effect of a plane-like reflector, (b) showing the effect of a vessel-like reflector.

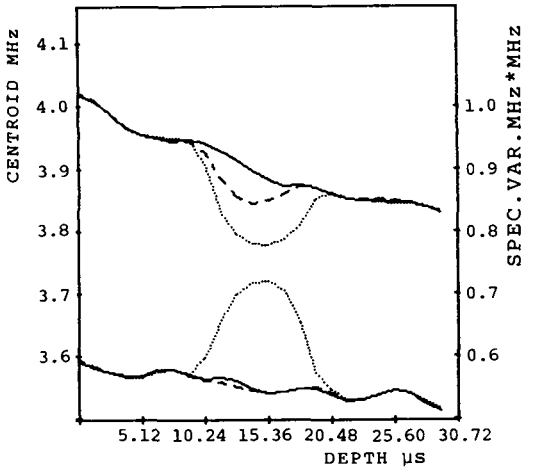

Fig. 2 Simulation : Running spectral centroid (upper curve) and spectral variance (lower curve) averaged on 32 simulated A-lines. Solid line : homogeneous medium. Dashed line : corresponding to figure 1a. Dotted line : corresponding to figure 1b.

influence of the specular reflector on equidistant time windows sampling different A-lines.

On calculating the running spectra through the Short Time Fourier Analysis algorithm, the range resolution is limited by the time window duration : the specular reflector noise affects the running spectral moments on a duration equivalent to the window duration.

The distortion visible on the running spectral centroid and variance are mainly due to the frequency content of the specular echo. The low spectral centroid values corresponding to the reflector (plane-like or vessel-like reflector) is characteristic of the scattering by large structures. The amplitude effect (i.e. the local variation of energy due to a specular echo) induces very little change in the evolution of the running spectral moments. The effect on the spectral centroid is more important for the vessel-like reflector and in the same way, an interesting effect on the spectral variance must be noticed. In that case, the spectral variance is affected by an important specular echo noise, when no noise is perceptible on the spectral variance in case of a plane-like reflector. Referring to the first part, this can be attributed to the non-random interferences. Both sign and amplitude of such non-random interferences noise depends on the distance between the two interfering echoes.

2) Experimental results

a) Data acquisition system

The experimental system used for data acquisition on phantom materials and in vivo muscle is composed of :
- a commercial type echograph (EDAP 10) supplied with a mechanical scanning focused single element transducer (focus : 90 mm, center frequency : 5 MHz)
- an 8 bit, 25 MHz A/D converter (DATA 6000).
- a microcomputer (WICAT) for data storing and processing. Our data base on phantom material consists of rf lines of 2048

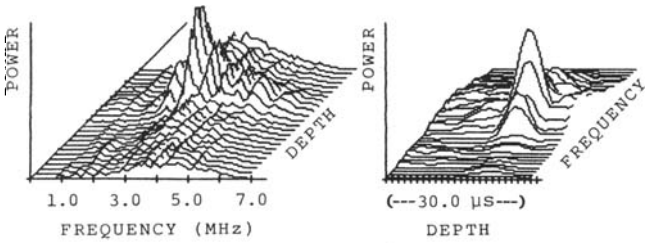

Fig. 3 Phantom : Running power spectra averaged on 64 simulated A-lines recorded for a foam phantom including a vessel-like reflector.

points (about 6 cm). The data base on in vivo muscle consists of 1024 points rf lines.

b) Phantom material

The phantom material is a foam phantom and the vessel-like reflector within the foam is a 1.1 mm diameter catheter. The running spectra ensemble-averaged on 64 lines, in presence of the reflector are presented on figure 3. The corresponding running spectral centroid and variance, compared with the results obtained on the foam phantom once the reflector has been withdrawn, are shown in figure 4. Good agreement is found between experimental (Figs. 3,4) and simulated (Figs. 1b, 2) curves. The deterministic interference noise due to the vessel-like structure of the catheter is particularly visible on the running spectra and on the running spectral variance (Figs. 3, 4).

c) In vivo measurements

When we started our data acquisition on in vivo muscle (Vastus medialis) in order to estimate the slope of attenuation, we found that the running spectra and the running spec-

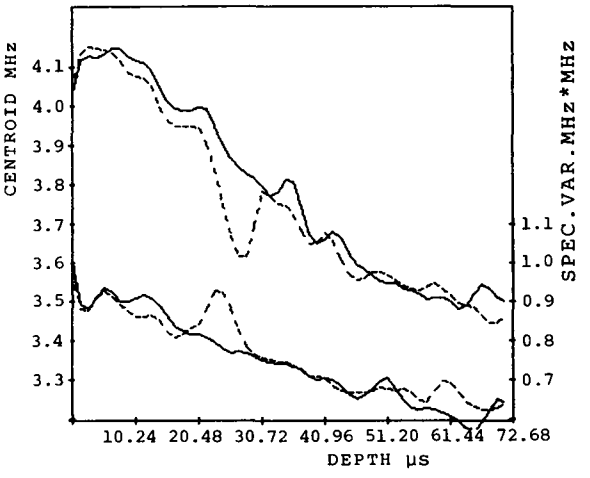

Fig. 4 Phantom : Running spectral centroid (upper curve) and spectral variance (lower curve) averaged on 64 A-lines. Solid line : foam phantom without obstacle. Dashed line : foam phantom with vessel-like reflector.

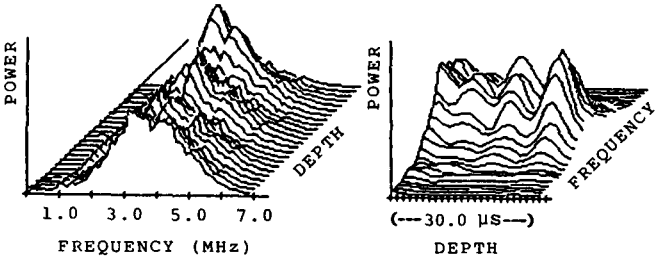

Fig. 5 In vivo muscle : Example of running spectra averaged on 32 A-lines recorded on in vivo muscles.

tral centroid were noisy even after averaging of a significant number of spectra (Figs. 5,6). This means that the lines of a scan were correlated and it had to be interpreted as a specular echo effect. The pattern of the running spectra and of the running spectral centroid and variance, when compared to the simulated curves (Figs. 1,2) can be interpreted as being characteristic of a plane-like reflector.

These reflectors within the muscle were identified as being made of connective tissues (aponeurosis) which simulate small reflecting planes of any orientation and any size.

d) Attenuation and specular reflectors

The importance of specular echo noise when estimating the slope of attenuation with a spectral centroid shift method should be emphasized. In the situation illustrated in figure 6, the reflector location is at the end of the data segment. The linear fit of the curve of the spectral centroid will deliver an overestimated value for the slope of attenuation due to the low frequency content of a specular echo. On the contrary, if the specular echo were located at the beginning of the data segments, then the bias introduced in the attenuation measure-

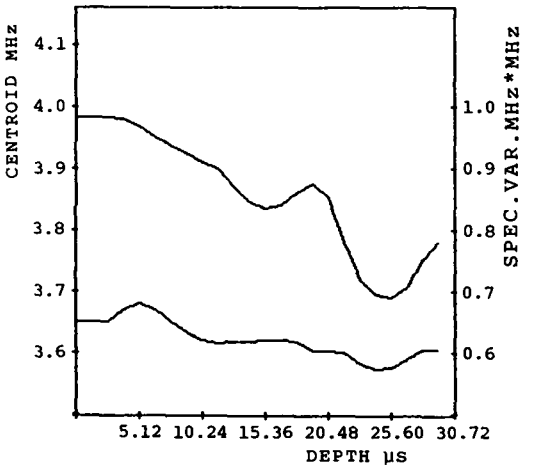

Fig. 6 In vivo muscle : Spectral centroid and variance vs. time corresponding to figure 5.

ment would be of the opposite sign and would provide for an underestimated value of the attenuation slope. This is summarized in table I where the results of attenuation measurements in the foam phantom with and without the reflector are reported. The estimation of the slope of attenuation has been done by considering 1024 points data segments including the specular echo either at the end or at the beginning of the data segments.

IV. INFLUENCE OF SPECULAR ECHOES IN A NARROW BAND TECHNIQUE

1) Phantom

We plotted in figure 7a the attenuation coefficient values (dB/cm) vs. frequency for the foam phantom with and without the reflector. One must keep in mind that, in this technique, the spatial information is lost since the attenuation values are obtained after a linear fit through the log-power spectra values at each frequency. The attenuation coefficient values plotted in figure 7a are obtained by processing the 2048 points of the rf signal, which represent the whole A-line. In this case, the specular echo is located at about the middle of the lines, and there is very little difference between the two curves. However, the results are quite different whenever the linear fit is done on the running spectra corresponding to only 1024 points data segments. In this particular case, we must examine separately two possible situations for the specular echo : either at the beginning, or at the end of the segments.

In figure 7b are plotted the frequency-attenuation curves of the foam phantom after a linear regression fit of log-power spectra corresponding to 1024 points data segments including the specular echo at the end. In this case, the specular echo produces a maximum of energy at the end of the running spectra and so yields an underestimated decay of the log-power spectra at each frequency. Thus, the frequency-attenuation curve corresponding to the foam phantom including the reflector is below the frequency-attenuation curve corresponding to the foam phantom. Moreover, as the specular echo is a low frequency effect, the deviation between the two regression lines plotted in figure 7b increases towards the low frequencies.

This narrow band technique is very sensitive to local variations of amplitude (or energy). Indeed, the nonrandom interferences producing scalloping on the averaged spectra are still visible on the frequency-attenuation curve of figures 7b and 7c. Figure 7c shows the frequency-attenuation curve for the foam phantom including the reflector together with the power spectrum corresponding to the reflector position. The scalloping of the power spectrum is reproduced on the frequency-attenuation curve.

In contrast, the specular echo effect is reversed whenever the reflector is at the beginning of the data segments as shown in figure 7d. In that case, the location of the local maximum of energy at the beginning of the running spectra yields attenuation coefficients exceeding the actual values. The scalloping is still visible on the curve.

2) In vivo measurements

Figures 8a, 8b and 8c illustrate the specular echo effect in two different situations with in vivo data. They show two different 32 A-line muscular scans (same person, same

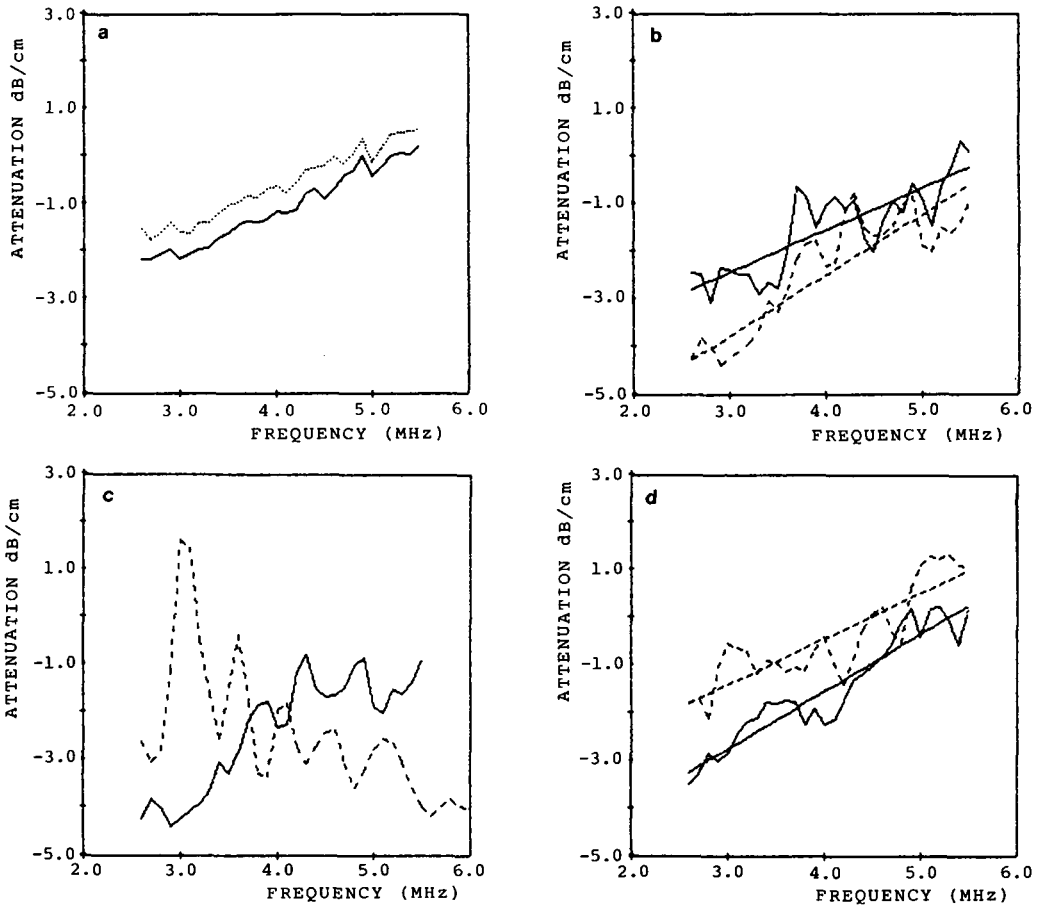

Fig. 7 Phantom: Frequency-attenuation curves in the foam phantom without the reflector (Solid line), with the specular reflector (dashed line).
(a): Attenuation values obtained by linear fitting through the power spectra corresponding to 2048 points A-lines
(b): Attenuation values obtained by linear fitting through the power spectra corresponding to 1024 points A-lines specular echo located at the end of the lines
(c): Power spectra (dashed line) of the windowed signal including the specular echo, together with the frequency attenuation curve (solid line) of figure 7b.
(d): same as (b) except the specular echo located at the beginning of the lines.

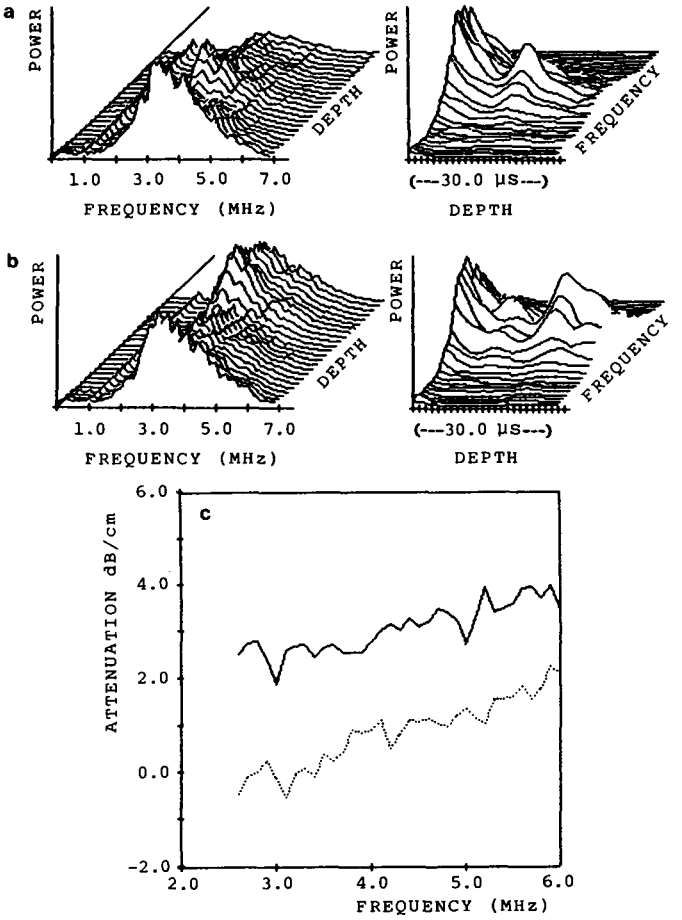

Fig. 8 In vivo : (a) and (b) Example of running spectra in two different muscular planes. (c) frequency-attenuation curves, solid line corresponding to figure 8a. and dotted line corresponding to figure 8b.

muscle) and the influence of the specular reflector location on the in vivo frequency-attenuation curve.

3) Attenuation and specular reflectors

As mentionned above for attenuation measurements with a spectral centroid shift method, the specular echo introduces also a bias on the attenuation slope estimates with the narrow band technique. Referring to table I, we see that the sign of the introduced bias depends on the location of the echo.

The amplitude effect is more perceptible in a narrow band technique than in a spectral centroid shift technique. The estimation of the attenuation coefficient at one frequency may be meaningless, because of the on Y-axis shift of the frequency-

Table I: Slope of attenuation in the foam phantom including a specular reflector. The calculation was performed using 1024 points of rf signal. (1): Specular echo located at the end of the data segments, (2): echo located at the beginning of the data segments.

	CENTROID SHIFT (dB/cm MHz)	NARROW BAND (dB/cm MHz)
(1)	1.55	1.65
(2)	0.98	0.82

attenuation curve. This shift in the attenuation coefficient values is far from being negligible as can be seen in figures 7a and 7d ; the on Y-axis shift is about 1 dB/cm at 4 MHz. It must be kept in mind that, due to the specular echo effect, the apparent frequency-attenuation law is

$$A\ (dB/cm) = A_o + \beta f^n. \qquad (8)$$

(Note that a similar effect occurs when using non-constant amplification vs. time of the rf signals. The frequency-attenuation curve will be vertically shifted according to the amplification slope.) If the attenuation law should be measured with the two parameters β_o : slope of attenuation and n : frequency exponent, the A_o value must be estimated and corrected for.

V. PROCEDURES FOR MINIMIZING THE SPECULAR ECHO NOISE

1) Algorithm for data correcting

An algorithm for specular echo detection and data correction is possible if specular echo amplitude is greater than the mean amplitude of the backscattered echoes of the Rayleigh scatterers. Under this condition, the specular echo can be detected on rf echographic response by means of simple amplitude detection. The first step is to compare the amplitude of the rf signals to the amplitude of a time-decreasing exponential (Fig. 9a). The exponential should for example express the decay of signal amplitude caused by the attenuation in the medium at the emitted center frequency (Of course, the comparison will be significant only if constant gain is applied to the whole duration of rf data segments). In the second step, a time window is centered on the maximum amplitude of the detected echo, within which the points are set to the zero value (Fig. 9b). The next step performs the restitution of the rf signal in place of the supressed echo in the following manner : the first half of the zero-value points is replaced with the immediately preceding equivalent length of rf signal. This is realized by folding the rf signal around the first point set to the zero value (Figs. 9b, 9c). In the same way, the second part of the zero-value points is replaced with the immediately following rf signal. Figure 9 illustrates algorithm on a 512-point data segment from the foam phantom.

Figure 10 presents the running spectral centroid and variance before and after data correction and shows the effi-

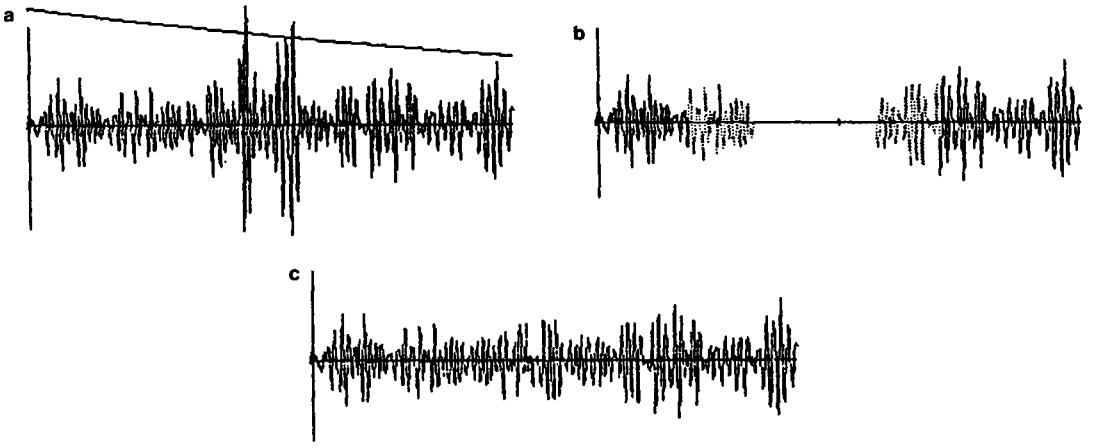

Fig. 9 Algorithm for correcting the data from the specular echo noise. (a) Signal before correction. Echo detection with a decreasing exponential.
(b) Suppression of the specular echo. In dotted line the part of the rf signal used to fill the zero value points.
(c) Signal after correction.

ciency of the algorithm in detecting a single specular reflector embedded in a homogeneous medium. Although the situation in muscle is somewhat different, the degree of heterogeneity in muscular tissues being much more important than in the studied phantom where feasability is demonstrated, we are at present studying the possibility for correcting in vivo data using this algorithm.

2) Data averaging

Another technique for minimizing the specular echo noise is to specify an appropriate data acquisition procedure,

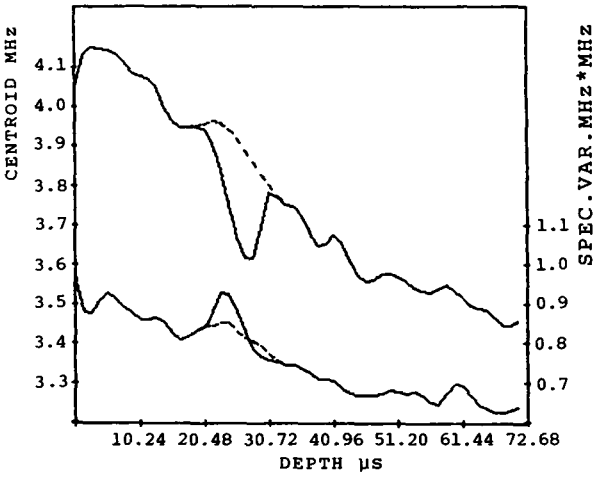

Fig.10 Phantom : Effect of the correction algorithm on the spectral centroid and variance. Solid line : before correction. Dashed line : after correction.

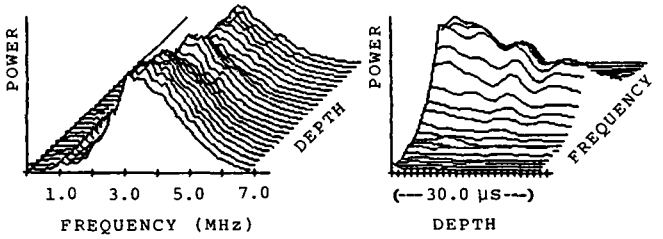

Fig. 11 In vivo muscle : running spectra averaged on 256 A-lines. The lines are obtained by scanning 8 different muscular planes each with 32 lines.

based on scanning a larger tissue volume, in order to be sure of acquiring uncorrelated A-lines. This is shown in figures 11 and 12. The running spectral centroid and variance are plotted after averaging the spectra on 256 lines recorded in 8 different muscular sections, each containing 32 lines. The effect of averaging is quite appreciable in diminishing the specular echo noise. However, this technique increase the volume of necessary data as well as the acquisition and processing times. Moreover, it needs a minimum tissue volume for insuring statistical convergence.

VI. CONCLUSION

Two types of algorithm, both based on short time fourier analysis, provide theoretically for an estimation of the slope of attenuation (dB/cm.MHz) : the spectral centroid shift method and the narrow band method. The reliability of the estimators depends on the homogeneity of the medium investigated. Nevertheless, heterogeneities in the medium can result in a depth-dependent or frequency-dependent response of the medium, which makes the estimation much more complicated.

We show that specular reflectors, as can be found in muscle, induce a correlation between the A-lines sharing a

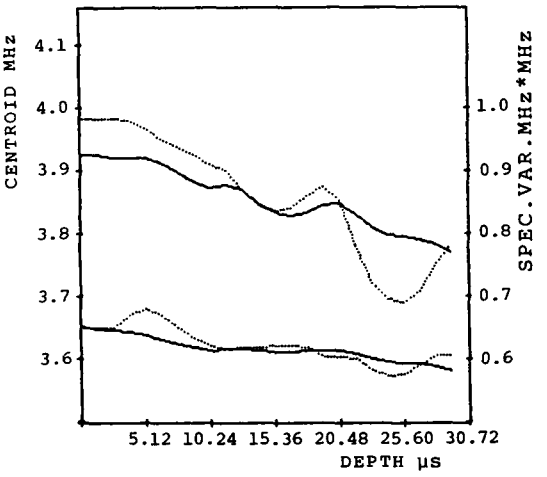

Fig. 12 In vivo muscle : Effect of averaging on 256 lines on the centroid and variance vs. depth. (solid line). Effect of averaging on 32 lines of one muscular plane is shown in the dotted line.

common reflector. This appears as a distortion in the running spectra and the running spectral moments. As could be expected from scattering theory, specular reflectors show a low frequency behaviour. The specular echoes, on the other hand, induce a significant vertical shift of the frequency-attenuation curve obtained from the narrow band method. As a consequence the attenuation coefficient (dB/cm.MHz) extrapolation at the zero frequency value must be considered very carefully, as it is strongly dependent on specular echo noise.

We point out also the bias introduced by specular echo noise in the estimation of the slope of attenuation. This bias depends on the reflector location on the data segment and on its size. A way of minimizing the specular echo noise might be to select A-lines without specular echoes either during the data acquisition or before the data processing. However, as a minimum amount of data is required for the statistical convergence of the estimation, such a solution could hardly be applied to muscular investigations due to the large degree of heterogeneity in muscular tissues. Thus, we proposed two methods for diminishing the importance of the specular echo noise :

a) Automatic detection and correction of the specular echoes in the rf signal. One should also keep in mind that $specular reflectors might have a low intensity of reflectivity and so cannot be detected easily by such an algorithm.

b) Acquisition of a great number of A-lines in various muscular planes and averaging of the corresponding data. This leads to a reliable estimation of the slope of attenuation but actually needs a large volume of data and so allows the estimation of the attenuation slope only in large organs.

The two procedures (algorithm or averaging) that we developed for attenuation measurements in vivo muscles may be applied also to other in vivo situations.

REFERENCES

[1] Kuc, R., Clinical application of an ultrasound attenuation coefficient estimation technique for liver pathology characterization, IEEE Trans. Biomed. Eng. BME-27, 312-319 (1980).

[2] Maklad, N.F., Ophir, J., and Balsara, V., Attenuation of ultrasound in normal liver and diffuse liver disease in vivo, Ultrasonic Imaging 6, 117-125 (1984).

[3] Wilson, L.S.,Robinson, D.E., and Doust, B.D., Frequency domain processing for ultrasonic attenuation measurement in liver, Ultrasonic Imaging 6, 278-292 (1984).

[4] Ophir, J., Maklad, N.F., and Bigelow, R., H., Ultrasonic attenuation measurements of in vivo human muscles, Ultrasonic Imaging 4, 290-295 (1982).

[5] Kuc, R. and Schwartz, M., Estimating the attenuation slope for liver from reflected ultrasound signals,IEEE Trans. Sonics Ultrasonics SU-26, 353-362 (1979).

[6] Ophir, J. and Maklad, N.F., A New Stochastic C.Scan Technique of Attenuation Coefficient Measurement in Tissue Equivalent Material, in Proc. 23rd Ann. Mtg. AUIM, p.118 (Amer. Inst. for Ultrasound in Med., Bethesda, MD, 1978) Abstract Only.

[7] Flax, S.W., Pelc, N.J., Glover, G.H., Gutman, F.D., and Mclachlan, M., Spectral characterization and attenuation measurements in ultrasound, Ultrasonic Imaging 5, 95-116 (1983).

[8] Hottier, F. and Bernatets, J.L., Estimation of ultrasonic attenuation in biological tissues, Acta Electronica 26, 33-58 (1984).

[9] Berger, G. and Perrin, J., Attenuation Principles and Measurements for Tissue Characterization in Ultrasonic Tissue Characterization : Clinical Achievement and Technological Potentials, J.M., Thijssen, ed., pp. 177-185 (Staffleu's Scientific Publishing Company, Alphen a/d Rijn, Holland, 1980).

[10] Fink, M., Hottier, F. and Cardoso, J.F., Ultrasonic signal processing for in vivo attenuation measurements : short time fourier analysis, Ultrasonic Imaging 5, 117-135 (1983).

[11] Cloostermans, M.J.T.M. and Thijssen, J.M., A beam corrected estimation of the frequency dependent attenuation of biological tissues from backscattered ultrasound, Ultrasonic Imaging 5, 136-147 (1983).

[12] Cardoso, J.F. and Fink, M., Diffraction Correction in Echographic Attenuation Measurements, in 1983 IEEE Ultrasonic Symposium Proceedings, PP. 841-846. (IEEE Cat. N°83 CH 1947-1).

[13] Fink, M. Cardoso, J.F., and Laugier, P., Diffraction effect analysis in medical echography, Acta Electronica 26, 59-80 (1984).

[14] Laugier, P., Berger, G., Fink, M., and Perrin, J., Influence of specular relectors on attenuation measurements on muscles, Ultrasonic Imaging 7, 84 (1985). Abstract only.